Evaluation of aerosol optical depth for further assimilation into WRF-Chem simulations

Dunia Bachour[1], Daniel Perez-Astudillo[1], and Christos Fountoukis[1]

[1] Qatar Environment and Energy Research Institute, HBKU, Doha (Qatar)

Abstract

WRF-Chem is a powerful simulation tool for modeling atmospheric parameters and processes that influence solar radiation reaching the Earth's surface. By integrating aerosols and their interactions with radiation, WRF-Chem provides estimates of solar radiation reaching the surface that can be used as valuable information for solar energy forecasting. However, the prediction of solar radiation comes with high uncertainties related to the high variability of atmospheric components, especially aerosols in clear-sky conditions. In this contribution, the aerosol optical depth (AOD) parameter is used to represent the optical property of aerosols. AOD derived from WRF-Chem and a reanalysis model (CAMS) are evaluated in comparison to ground AOD data. The resulting analysis will server to correct the forecasted WRF-Chem AOD products and thus the prediction of solar radiation based on additional analysis of AOD data in a region with mostly cloudless conditions in general, but with the presence of aerosols and airborne desert dust throughout the year.

Keywords: WRF-Chem, aerosols, AOD, CAMS, direct normal irradiance

1. Introduction

The WRF-Chem model is a powerful numerical weather prediction (NWP) simulation tool for modeling atmospheric parameters and processes that influence solar radiation reaching the Earth's surface. It is a coupled model combining the weather forecasting capabilities from the Weather Research and Forecasting (WRF) model, as well as chemical transport capabilities that simulate the emissions, transport, and transformation of atmospheric gases and aerosols. WRF-Chem can be used as a valuable tool for solar radiation forecasting, with somehow large uncertainties, however, due to variability in clouds, in general, and in aerosols when clouds are absent (Ruiz-Arias et al., 2013). These uncertainties are even more pronounced on the direct solar radiation component, given its high sensitivity to the optical properties of the atmosphere, mainly coming from aerosols in cloud-free conditions (Gueymard, 2012). Among several parameters used to describe the aerosol optical properties, the aerosol optical depth (AOD) is commonly used to quantify the extinction of solar radiation by aerosols. AOD is acquired by ground-based sun photometers, such as the worldwide network of sun photometers provided by the AErosol Robotic NETwork (AERONET). Ground observations offer localized data of high quality; however, they are usually not available for long periods and suffer from data gaps. Other alternatives for AOD data retrieval are satellite products such as the Moderate Resolution Imaging Spectroradiometer (MODIS), or models such as NWP and global atmospheric chemistry models. Recently, atmospheric models, using data assimilation and reanalysis from satellite or ground observations, provide continuous time-series of AOD data with relatively high temporal resolution. The Modern-Era Retrospective analysis for Research and Applications, version 2 (MERRA-2), developed at NASA, and the Copernicus Atmosphere Monitoring Service (CAMS) model, developed at the European Centre for Medium-range Weather Forecasting, are two examples of reanalysis models widely used in solar resource applications to derive AOD data.

In this contribution, AOD derived from CAMS and WRF-Chem model will be evaluated in comparison to ground AOD data, to assess the reliability of the derived data in Doha, Qatar, a region characterized by high concentrations of atmospheric dust. The results of the analysis will be used to study a possible correction on WRF-Chem AOD products in high aerosol loads conditions, which may improve WRF-Chem performance in predicting solar radiation when further analysis of AOD data is performed.

Selection and/or peer review under responsibility of Scientific Committee
10.18086/eurosun.2024.10.02 Available at http://proceedings.ises.org

2. Methodology

A high-precision monitoring station equipped with thermopile sensors is used here to collect ground-measurements of the direct, global and diffuse components of solar radiation.

At the same site, a sun photometer is used to derive ground AOD data, based on a spectrally selective detector measuring the spectral extinction of the direct radiation from the top of the atmosphere to the radiation at the earth surface for several wavelengths. The total optical depth is derived following the Lambert-Beer equation and AOD is derived from the total optical depth after removing the contribution of the other extinctions including the molecular scattering, ozone and other trace gas absorptions. To conform with satellite-derived data, the 500 nm channel is used here; this is also the closest wavelength to the representative wavelength (550 nm) of the scattering properties of aerosols in the atmosphere.

In this study, the three-dimensional WRF-Chem meteorology-chemistry model was implemented over the Arabian Peninsula, with a focus on enhanced grid resolution specifically for Qatar. The model simulated three primary processes: the emission of atmospheric components (both gases and aerosols), their transport, and their physicochemical transformations in the atmosphere. It was applied to the Middle East region using a 3-D grid system within a two-way nesting configuration, allowing communication between three domains with varying grid resolutions, all of which ran concurrently (Fountoukis et al., 2022). Aerosol concentration data moved in and out of all computational domains during model integration. The parent domain utilized a 50 km × 50 km grid resolution, while the intermediate nested domain (centered on the Arabian Desert) used a resolution of 10 km × 10 km. The third domain, covering Qatar, was resolved at 2 km × 2 km. The GOCART (Georgia Institute of Technology–Goddard Global Ozone Chemistry Aerosol Radiation and Transport) aerosol scheme was employed in all simulations, alongside the RACM (Regional Atmospheric Chemistry Mechanism) scheme for chemistry. The HTAP (Hemispheric Transport of Air Pollution emissions; http://www.htap.org/) anthropogenic emissions were used, featuring a grid resolution of 0.1° × 0.1°. Dust emissions were simulated using the US Air Force Weather Agency (AFWA) scheme, which incorporates the MB95 dust emission parameterization with typical airborne dust size distributions. Initial conditions for all pollutant concentrations are taken based on typical measurements of air quality in the region.

AOD is also derived from the reanalysis products CAMS. The CAMS Radiation Service v4.6 all-sky irradiation is used to derive 1-minute AOD values at 550 nm as the sum of all available optical depth products, and from these, hourly-averaged AOD values are calculated.

The statistical parameters used to compare the modeled and ground AOD data are the mean bias error (Bias) and the root mean square error (RMSE). For each entry, the difference and its square between the estimated (AOD WRF and AOD CAMS) and measured (AOD Ground) at the same time stamps (t) are calculated for the corresponding period. Then, these differences and their squares are summarized to determine the corresponding bias and root mean square error. The values are also expressed in relative values with respect to the mean values calculated from the measured AOD. Equations 1 to 6 are used to determine the statistical parameters where N is the total number of considered values.

$$\Delta_{(t)} = AODestimated_{(t)} - AODground_{(t)} \quad \text{(eq.1)}$$

$$Bias = \frac{\sum_1^N \Delta_t}{N} \quad \text{(eq.2)}$$

$$RMSE = \sqrt{\frac{\sum_1^N {\Delta_t}^2}{N}} \quad \text{(eq.3)}$$

$$mean\ AOD = \frac{\sum_1^N AODground(t)}{N} \quad \text{(eq.4)}$$

$$rBias = \frac{Bias}{mean\ AOD} \quad \text{(eq.5)}$$

$$rRMSE = \frac{RMSE}{mean\ AOD} \quad \text{(eq.6)}$$

3. Results

3.1 Ground AOD

To quantify and study the range of AOD values seen in Doha's conditions, we study in figure 1 the hourly variations of AOD derived by the sun photometer for a period of ~one year, showing all months consecutively excluding August due to the unavailability of processed data for this month at the time of analysis. Note that the months are shown in order from January until December for clarity, although the included January and February corresponds to year 2023 while the other months are in year 2022. The blue lines on the figure correspond to the beginning of a new month. For some months AOD variation is confined within a defined band, while for other months the variation is more obvious with an observed high range (between 0.3 and 1.4 in July for instance). The observed AOD mean is ~ 0.5 with a standard deviation of 0.27, indicating a dynamic fluctuation of AOD in the region with a more turbid atmosphere in the summer season. This variation in AOD induces a pronounced variation in solar radiation; when simulating the beam normal irradiance component with SMARTS2 (Simple Model of the Atmospheric Radiative Transfer of Sunshine) model, the maximum is reduced by ~ 5 % when AOD is 0.1, and by ~ 50 % when AOD is equal to 1, with respect to AOD = 0 (Bachour et al., 2023).

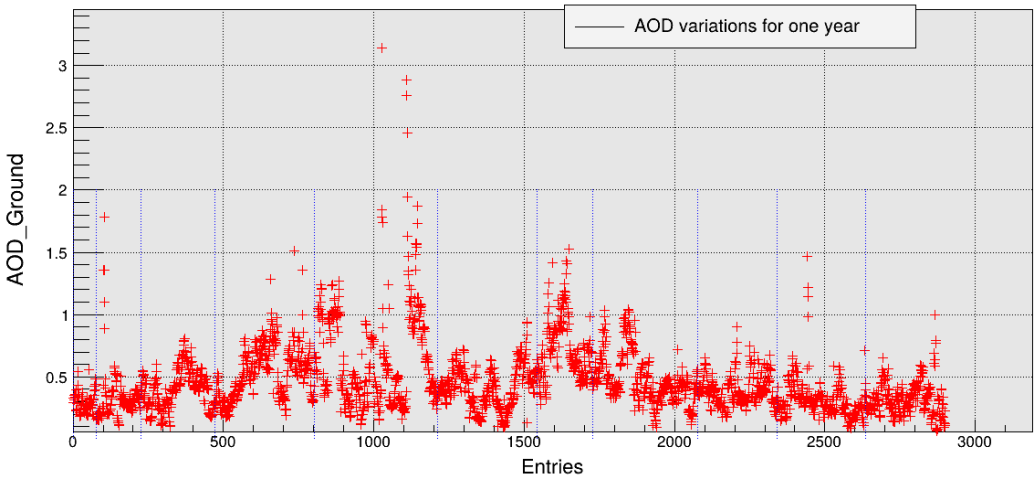

Figure 1. Variations of hourly AOD through one year, measured by a sun photometer in Doha, Qatar.

3.2 Model-derived AOD

Hourly AOD data were also derived from the CAMS reanalysis database and WRF-CHEM. Figure 2 shows an example of the normalized frequency distributions of AOD from these models in comparison with the ground data for two months: May, and July 2022.

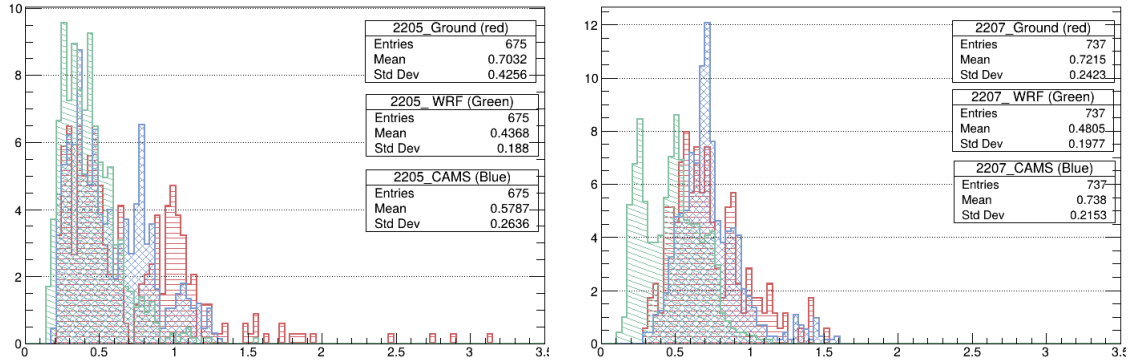

Figure 2. Normalized frequency distribution (in %) of hourly AOD per month.

Looking to the overall distribution, AOD values obtained from CAMS (blue line) agree partially with AOD obtained from the ground (red line), with differences observed mainly in the tail part of the two histograms, where higher AOD values are being captured by the ground measurements. AOD values between 0.7 and 1 are frequent in the CAMS data; AOD higher than 1, values attributed to local dust events, are observed in the

ground measurements. For WRF-Chem, the distribution of modeled AOD (green line) does not conform with the ground-derived values, with an observed underestimation. A clear discrepancy is seen towards the low AOD values where WRF-Chem reports very low values with high frequency (even for other months not shown here), which may not be possible in the turbid atmosphere of Doha. WRF-Chem is clearly not able to capture high AOD values, with mean values significantly lower than those derived by the sun photometer, highlighting the model limitations when predicting AOD in Doha's desert environment (Fountoukis et al., 2020), and the need to reconfigure or correct the model with new parameters based mainly on AOD, in order to improve the ability of WRF-CHEM to predict local dust events in a desert environment, consequently improving the prediction of solar radiation in a desert location with high aerosol loads.

To examine the comparison in more detail, the profile of the hourly AOD data from the 3 sources is plotted at the same time stamps for two one-month periods (May and July of 2022): CAMS and ground data in Figure 3, WRF-Chem and ground data in Figure 4. The data of the x-axis, labeled as 'entries' in the plots, are chronologically sorted but they are not consecutive in time, and they include commonly available AOD data from both sources at the same timestamp. The dotted red vertical lines are plotted to discern the first entry of a new day. The statistical comparison with the ground data is reported in table 1 for CAMS and table 2 for WRF-Chem; the mean bias error (Bias) and the root mean square error (RMSE) are determined, respectively, by calculating the differences and their squares between the modeled and ground AOD values at the same time stamps, and their corresponding mean Bias and RMSE and their relative values (rBias, rRMSE) with respect to the mean values of AOD-Ground. The number of data points in the comparison is also shown in the tables.

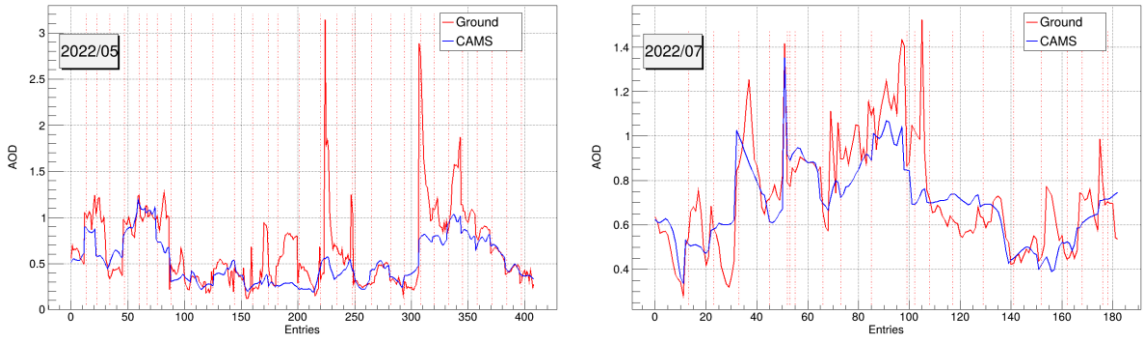

Figure 3. Hourly AOD variations of CAMS in comparison with ground data in Doha, Qatar.

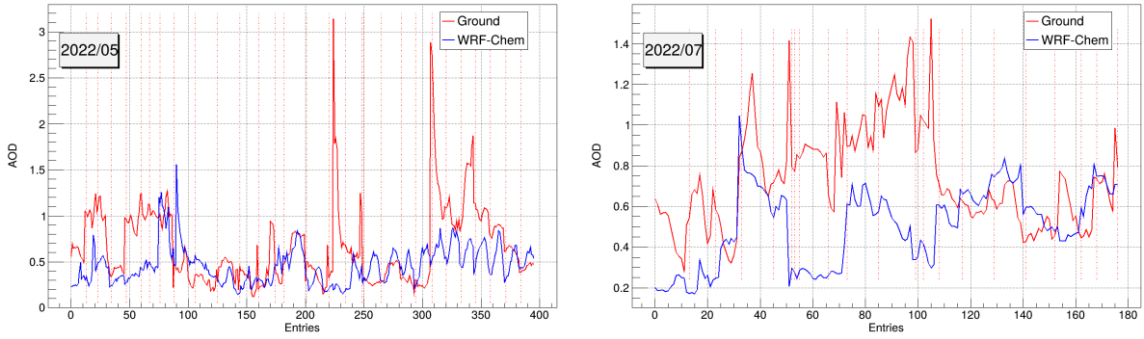

Figure 4. Hourly AOD variations of WRF-Chem in comparison with ground data in Doha, Qatar.

Table 1. Comparison of AOD CAMS and ground.

MONTH	BIAS	RBIAS (%)	RMSE	RRMSE (%)	DATA POINTS
05/22	-0.15	-20.81	0.34	49.2	340
07/22	-0.03	-4.44	0.16	22.4	176
09/22	-0.04	-8.27	0.12	25.28	322
02/23	0.03	7.95	0.22	66.99	145

Table 2. Comparison of AOD WRF-Chem and ground.

MONTH	BIAS	RBIAS (%)	RMSE	RRMSE (%)	DATA POINTS
05/22	-0.23	-31.69	0.49	68.51	327
07/22	-0.22	-30.51	0.38	51.87	170
09/22	-0.2	-41.81	0.29	59.75	322
02/23	-0.09	-29.10	0.26	79.43	145

From figures 3 and 4, it is observed that CAMS captures better the local variability observed in the ground data, with larger discrepancies observed in WRF-Chem data. However, high AOD values observed in the ground data are not properly modeled by either CAMS or WRF-Chem. When comparing the statistics for each of the months in tables 1 and 2, CAMS is mostly underestimating the AOD values with a relative bias less than 10 % except for May. For WRF-Chem the AOD values are underestimated for all the months and the relative RMSE is considerably high.

3.3 Data validation

The solar radiation measurement is used For AOD data validation; the measured direct component, Gb, is compared with a clear-sky Gb (Gb_cs) calculated with the European Solar Radiation Atlas (ESRA) clear-sky model, with a Linke turbidity value of 1 to get the maximum Gb representing a perfectly clear atmosphere free from any aerosols or water vapor. This component is then reduced by the AOD parameter to obtain Gb_cs, which quantifies the reduction in solar radiation caused by aerosols. See Equation 1 for more details, where m is the air mass and AOD is the value derived from ground, CAMS, and WRF-Chem.

Gb_cs = Gb-ESRA (max) * Exp (-m*AOD) (Eq.1)

Figure 5 shows an example of 3 daily profiles of measured (red line) and modeled Gb, as described previously. It is observed that Gb modeled using ground AOD data as input follows the measured Gb, while Gb modeled using AOD from CAMS and WRF-Chem deviates from the measured Gb with a significant overestimation due to an underestimation of AOD values. For a broader validation, the scatter plot of one month of data between the measured and modeled Gb shows a reasonably good agreement when using AOD data derived from the ground measurement (Bachour et al., 2023).

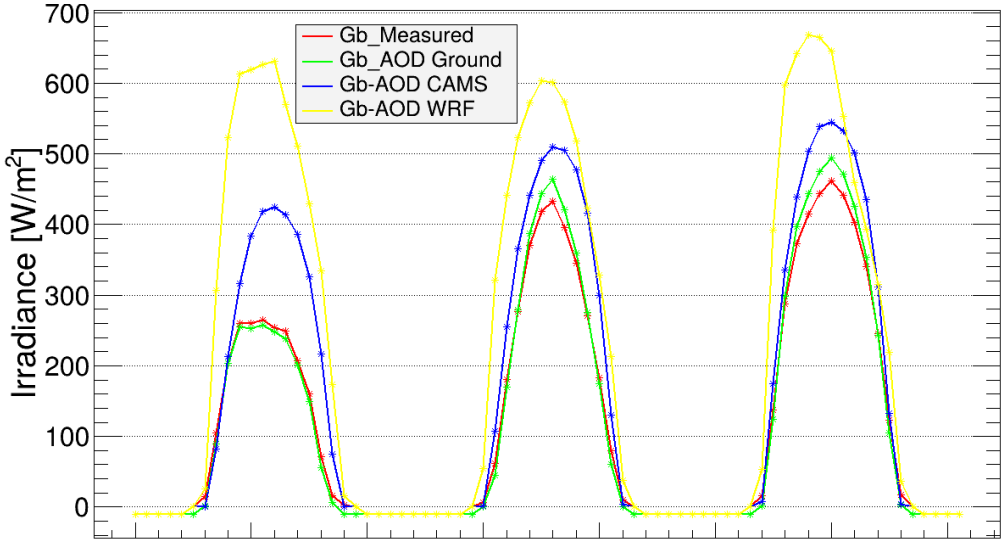

Figure 5. Daily profiles of measured and clear-sky DNI.

3.4 Data filtering

Although the processing of the sun photometer data includes a cloud screening algorithm that identifies cloudy periods and flags the corresponding AOD data, some days with relatively high AOD values identified from figures 3 and 4 will be further analysed to eliminate the possibility of outliers in the ground AOD data, which

may indicate cloud contamination and thus inaccurate ground AOD values. For this analysis, the direct solar radiation component Gb measured by a solar monitoring station located close to the sun photometer will be analysed. Although it is not straightforward to distinguish between the attenuation in Gb caused by clouds or aerosols without using additional data, days with clouds exhibit a profile with sharp decreases and recoveries as compared to the aerosol effects that tend to cause a more gradual reduction in irradiance throughout the day. Following this assumption, all days identified as days with possible clouds contamination are removed.

In addition, the cumulative distribution of the ground AOD has been analysed for each of the month; it was noted that AOD values less than 0.1 are extremely rare (<1% for all the studied months), and 0.14 are also quite rare (<1% for the studied months except for Feb, when it was ~ 3.5%). Table 3 shows the comparison excluding the suspected cloudy days. In addition to the exclusion of cloudy periods, tables 4 and 5 show the same parameters excluding also AOD data with values less than a fixed threshold: 0.1 in table 4 and 0.14 in table 5; only months with changes are reported.

Table 3. Statistical parameters between AOD WRF-Chem and ground, excluding cloudy periods.

Month	Bias	rBias	RMSE	rRMSE	Data Points
05/22	-0.22	-31.44	0.49	68.71	308
07/22	-0.16	-23.28	0.33	48	127
09/22	-0.19	-39.71	0.27	55.95	299
02/23	-0.02	-8.8	0.16	55.79	108

Table 4. Statistical parameters between AOD WRF-Chem and ground, excluding cloudy periods and AOD<0.1 .

MONTH	BIAS	RBIAS	RMSE	RRMSE	DATA POINTS
02/23	-0.02	-5.85	0.15	54.41	104

Table 5. Statistical parameters between AOD WRF-Chem and ground, excluding cloudy periods and AOD<0.14

MONTH	BIAS	RBIAS	RMSE	RRMSE	DATA POINTS
09/22	-0.19	-39.48	0.27	55.37	285
02/23	0.01	-0.1	0.15	49.85	76

From the bias values of the WRF-Chem, the model tends to underestimate the AOD values consistently. To keep consistency among all months, only periods with AOD values less than 0.1, seen only in WRF-Chem data, were eliminated as it is not ‘physically’ possible (not seen in the ground measurements during these months) in Doha’s conditions.

3.5. Correction of WRF-Chem AOD data

Since the WRF-Chem data consistently underestimated AOD, the bias correction method is used to improve forecasting results. This method consists of determining a mean bias error of the data within a certain period and using it to correct the forecasted results. The bias is calculated using the data of three months analysed together and used to correct the data of the remaining month (table 6).

Table 6. Statistical parameters for the comparison of ground and WRF-Chem AOD, using the bias correction method.

MONTH	BIAS	RBIAS	RMSE	RRMSE	DATA POINTS
05/22	-0.03	-5.47	0.42	64.25	356
07/22	-0.03	-4.47	0.28	42.10	131
09/22	-0.07	-14.15	0.2	41.84	317
02/23	0.14	50.44	0.21	73.59	107

While the bias of the forecasted data has been reduced for most of the tested months, their relative RMSE hasn't improved much, and the applied correction amplified the errors for February. This means that it is not adequate to apply the same correction on the forecasted results without considering some sort of data clustering based on data distribution similarity, or data seasonality. As a first attempt, looking to the frequency distribution of AOD WRF-Chem, a certain similarity is observed between months 5 and 7 (wider range with a relatively high mean of AOD values) compared to months 9 and 2 which show a somehow narrower distribution with lower mean AOD values. However, month 9 has a higher mean AOD value and exhibits

higher AOD variations than month 2. Table 7 shows the results of the bias correction method determined with the data of one month (i.e. month 5 and 9) and validated using the data of the similar month respectively (i.e. month 7 and 2), and vice versa. The errors for 5 and 7 are reduced, however the errors in months 9 and 7 are high as expected, suggesting the use of another correction factor for winter months with low AOD values.

Table 7. Statistical parameters for the comparison of ground and WRF-Chem AOD, using the bias correction method.

MONTH	BIAS	RBIAS	RMSE	RRMSE	DATA POINTS
05/22	-0.02	-2.47	0.42	64.06	356
07/22	-0.04	-5.37	0.29	42.2	131
09/22	-0.17	-35.87	0.25	53.27	317
02/23	0.16	59.6	0.22	80.15	107

Other correction methods are tested here and consist of finding a possible fit between two datasets, as will be defined in Figures 6 and 7, to check if errors improve compared to the bias correction method. Figure 6 shows an example of a scatter plot between AOD ground and WRF-Chem, with the x-axis presenting the WRF-Chem data and the y-axis presenting the ground data. The black line indicates the one-to-one line, while the red line represents the linear fit function found between the data, determined in the range 0 to 1.5 to eliminate some outliers, which might help the fit function to better represent the relation between the two datasets. Figure 7 shows the scatter plot between the point-by-point bias of WRF-Chem and ground AOD (y-axis) and AOD WRF-Chem (x-axis), and the fit function is shown with a solid red line. Following the same method discussed in the bias correction method, the fit functions are determined using the data of three months and validated using the data of the remaining month.

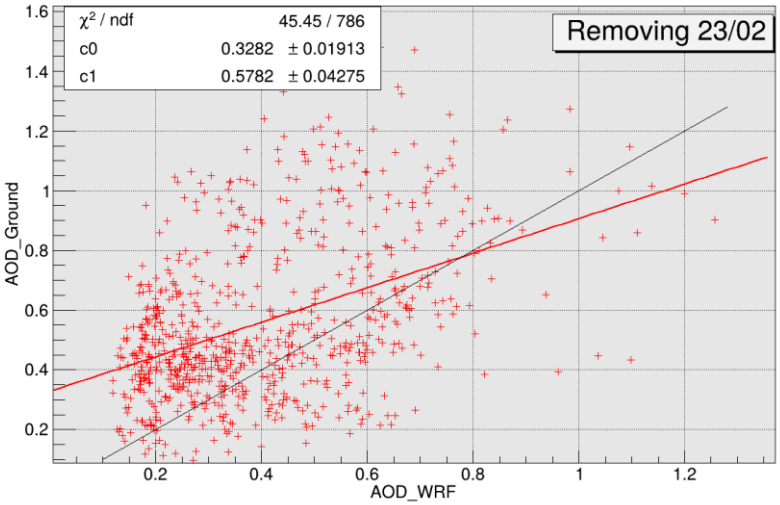

Figure 6. Scatter plot between measured and WRF-Chem AOD.

The linear fit function parameters (c0, c1) are determined from figure 6, in this case using the three months (5,7,9), and applied to correct AOD_WRF of month 2. The fit function is shown in equation 2. Table 8 shows the results of applying this correction on all forecasted AOD_WRF, alternating the used/removed months to have all possible combinations.

$$AOD\_ground = c0 + c1 * (AOD\_WRF) \qquad (Eq.2)$$

Table 8. Statistical parameters for the comparison of ground and WRF-Chem AOD, using the linear fit correction.

MONTH	BIAS	RBIAS	RMSE	RRMSE	DATA POINTS
05/22	-0.09	-13.69	0.42	63.89	356
07/22	-0.09	-12.58	0.27	39.87	131
09/22	-0.01	-3.18	0.17	37.21	317
02/23	0.2	70.68	0.23	82.3	107

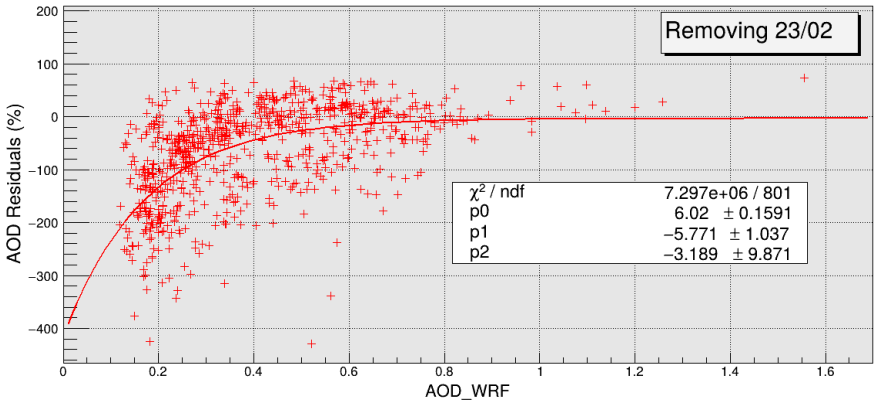

Figure 7. Scatter plot between bias and WRF-Chem AOD.

Figure 7 is used to determine the fit function between the residuals PR (as percentage of AOD_WRF), and AOD_WRF, following the formula shown in equation 3. The residuals are the differences between each AOD_WRF value and the corresponding ground-derived AOD.

$$PR = P2 - Exp\,(P0 + P1 * (AODWRF_{Chem})) \qquad \text{(Eq. 3)}$$

P2, P0, P1 are the fit parameters determined from the scatter plot using the data of three months. The correction is then applied on the remaining month comparing the calibrated WRF-chem AOD with ground data (table 9).

Table 9. Statistical parameters for the comparison of ground and WRF-Chem AOD, using the residuals correction.

MONTH	BIAS	RBIAS	RMSE	RRMSE	DATA POINTS
05/22	-0.26	-40.37	0.51	78.2	356
07/22	-0.22	-32.62	0.39	56.88	131
09/22	-0.30	-64.94	0.36	76.79	317
02/23	-0.12	-43.94	0.18	65.39	107

The results of the linear fit on AOD show a somewhat similar improvement as seen in the bias correction method; in some months the relative RMSE is even lower, thus reducing the dispersion of WRF-Chem data compared to the ground data, however the bias of the month of Feb is amplified similarly to the previous method, suggesting the need of aggregating the data by season following the sky turbidity level as discussed previously. The correction determined from the fitting of the residuals failed to improve the errors and in fact worsened them. This was expected looking to the wide band of data dispersion around the fit line (figure 7), reflected in the errors associated to the parameters of the fit (shown in the statistics box on the plot), mainly for P2.

4. Conclusions

Among different parameters used to quantify the aerosols, AOD is used to account for the attenuation of the solar radiation in the atmospheric column due to aerosols, and AOD quantification, whether short- or long-term, is required in many applications such as climate change, air quality, and solar radiation. Due to the high dynamicity of the aerosols in the atmosphere, AOD obtained by ground measurements remains the reference method for deriving reliable data with high temporal resolution, and models based on satellite observations and reanalysis databases provide AOD data with high uncertainties, mainly in regions with high aerosol loads.

In this contribution, AOD (with hourly temporal resolution) is quantified with a sun photometer deployed in Doha, Qatar to obtain ground-derived AOD data and evaluate the AOD products obtained from CAMS and WRF-Chem model. CAMS model data show relatively good agreement with the ground data. However, the assessment of the WRF-based data shows non-conformity and high discrepancy with the ground data, leading to the suggestion of correction methods to WRF-Chem reducing the errors of the forecasted values. By considering AOD post correction into WRF-Chem simulation process, the accuracy and reliability of the solar radiation prediction can be improved, mainly in region characterized by high concentrations of atmospheric dust.

5. Acknowledgments

Research reported in this work was supported by the Qatar Research Development and Innovation Council (Grant: ARG01-0503-230061). The content is solely the responsibility of the authors and does not necessarily represent the official views of Qatar Research Development and Innovation Council.

6. References

Ruiz-Arias, J.A., Dudhia, J., Santos-Alamillos, F.J., Pozo-Vázquez, D., 2013. Surface clear-sky shortwave radiative closure intercomparisons in the Weather Research and Forecasting model. Journal of Geophysical Research: Atmospheres 118, 9901–9913. DOI: 10.1002/jgrd.50778

Gueymard, C. A., 2012. Temporal variability in direct and global irradiance at various time scales as affected by aerosols. Solar Energy 86 (12), 3544–3553. DOI: 10.1016/j.solener.2012.01.013

Bachour, D., Perez-Astudillo., Fountoukis, C., Sanfilippo, A., 2023. Aerosols estimation in arid region for solar resource applications. EU PVSEC 2023 Conference Proceedings, 020364-001 - 020364-006. ISBN: 3-936338-88-4. DOI: 10.4229/EUPVSEC2023/4CO.9.4

Fountoukis, C., Harshvardhan, H., Gladich, I., Ackermann, L., Ayoub, M.A., 2020. Anatomy of a severe dust storm in the Middle East: Impacts on aerosol optical properties and radiation budget. Aerosol and Air Quality Research, 20, 155-165. DOI: 10.4209/aaqr.2019.04.0165.

Fountoukis, C., Mohieldeen, Y., Pomares, L., Gladich, I., Siddique, A., Skillern, A., Ayoub, M.A., 2022. Assessment of High-resolution Local Emissions and Land-use in Air Quality Forecasting at an Urban, Coastal, Desert Environment. Aerosol Air Qual. Res. 22, 220001. DOI: 10.4209/aaqr.220001